Scientific Research Publishing

Computational Chemistry, 2021, 9, 161-196
https://www.scirp.org/journal/cc
ISSN Online: 2332-5984
ISSN Print: 2332-5968

Investigation of the Antioxidant and UV Absorption Properties of 2-(2'-hydroxy-5'-methylphenyl)-benzotriazole and Its Ortho-Substituted Derivatives via DFT/TD-DFT

Numbonui Stanley Tasheh[1], Aymard Didier Tamafo Fouegue[2], Julius Numbonui Ghogomu[1,3*]

[1]Research Unit of Noxious Chemistry and Environmental Engineering, Department of Chemistry, Faculty of Science, University of Dschang, Dschang, Cameroon
[2]Department of Chemistry, Higher Teacher Training College Bertoua, University of Ngaoundéré, Bertoua, Cameroon
[3]Department of Chemistry, Faculty of Science, The University of Bamenda, Bamenda, Cameroon
Email: *ghogsjuju@hotmail.com

How to cite this paper: Tasheh, N.S., Fouegue, A.D.T. and Ghogomu, J.N. (2021) Investigation of the Antioxidant and UV Absorption Properties of 2-(2'-hydroxy-5'-methylphenyl)-benzotriazole and Its Ortho-Substituted Derivatives via DFT/TD-DFT. *Computational Chemistry*, **9**, 161-196.
https://doi.org/10.4236/cc.2021.93010

Received: June 7, 2021
Accepted: July 11, 2021
Published: July 14, 2021

Abstract

The demand and pursuit of chemical entities with UV filtration and antioxidant properties for enhanced photoprotection have been driven in recent times by acute exposure of humans to solar ultraviolet radiations. The structural, electronic, antioxidant and UV absorption properties of drometrizole (PBT) and designed ortho-substituted derivatives are reported via DFT and TD-DFT in the gas and aqueous phases. DFT and TD-DFT computations were performed at the M062x-D3Zero/6-311++G(d,p)//B97-3c and PBE0-D3(BJ)/def2-TZVP levels of theory respectively. Reaction enthalpies related to hydrogen atom transfer (HAT), single-electron transfer followed by proton transfer (SET-PT), and sequential proton loss electron transfer (SPLET) mechanisms were computed and compared with those of phenol. Results show that the presence of -NH2 substituent reduces the O-H bond dissociation enthalpy and ionization potential, while that of -CN increases the proton affinity. The HAT and SPLET mechanisms are the most plausible in the gas and aqueous phases respectively. The molecule with the -NH2 substituent (PBT1) was identified to be the compound with the highest antioxidant activity. The UV spectra of the studied compounds are characterized by two bands in the 280 - 400 nm regions. Results from this study provide a better comprehension antioxidant mechanism of drometrizole and present a new perspective for the design of electron-donor antioxidant molecules with enhanced antioxidant-photoprotective efficiencies for applications in commercial sunscreens.

Keywords

Antioxidant, Drometrizole, Density Functional Theory, Ultraviolet Absorption, Hydrogen Atom Transfer, Single Electron-Proton Transfer and Sequential Proton Loss Electron Transfer Mechanisms

1. Introduction

Biological systems depend on solar radiation for energy to sustain life. Unfortunately, chronic exposure to solar ultraviolet radiation (UVR) is responsible for health problems such as premature aging, erythema, skin cancers and sunburn [1] [2] [3] [4] [5]. Melanin (naturally occurring UV-absorbing pigment in the human skin) provides the first line of defense to the harmful effects of UVR but does not provide enough shield against high levels of UVR. To this effect, organic sunscreens are frequently used as photoprotectors [4]. Recently, attention has been shifted towards the use of sunscreens which in addition to the screening of detrimental UVR equally have photoprotection constituents [6]. Antioxidants efficiently serve this purpose, since they scavenge UV-induced free radicals [2] [7]. Flavonoids, polyphenols, resveratrol, etc., have been explored for such purposes. To qualify as a potential organic molecule for sunscreen applications, the molecule must be able to block UVR and scavenge resultant free radicals from UVR exposure [4] [8]. Knowledge of sunscreens comprising UV filters and antioxidant ingredients serve as a novel photoprotective strategy and research in this field is ongoing [3] [4] [6] [9].

2-(2'-hydroxy-5'-methylphenyl)-benzotriazole (PBT) commonly known as drometrizole (see **Figure 1**) is considered as a sunscreen ingredient and is utilized as a UV absorber and stabilizer [1] [10] [11]. Furthermore, it is known to

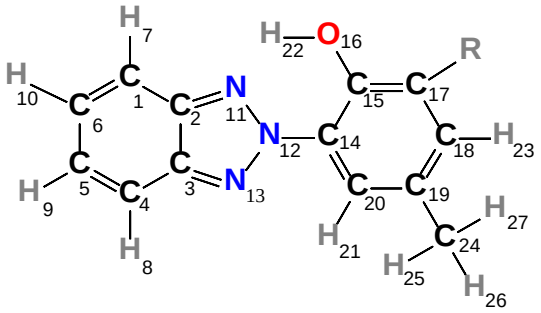

R	Abbreviations
-H	PBT or Drometrizole
-NH_2 (ED)	PBT1
-CN (EA)	PBT2

Figure 1. Schematic representation of PBT and its ortho-substituted derivatives with atomic numbering scheme (ED and EW represent electron-donating and attracting groups).

have antioxidant and stabilizing effects and has been approved as an indirect food additive [12]. Reference [1] reported that PBT is a potent Exited state intramolecular proton transfer (ESIPT)-mediated Non-linear optical (NLO) molecular switch which could be used as a chromophore. Despite all the studies on drometrizole from literature, there is no comprehensive theoretical study on the structure-antioxidant relationship as well as the antioxidant mechanism of drometrizole. Additionally, the presence of some substituents on PBT may enhance its antioxidant properties. Interestingly, electron-donating groups (EDGs) and electron-withdrawing groups (EWGs) are known to significantly affect the antioxidant activity of a phenolic antioxidant [13]. This insight has been a prime aid for the design and synthesis of new and more effective antioxidants [14]. Three major mechanisms to scavenge free radical by antioxidants have been recognized [15] [16]. These include hydrogen atom transfer (HAT), single-electron transfer followed by proton transfer (SET-PT), and sequential proton loss electron transfer (SPLET). The antioxidant activity of the phenolic antioxidants can be assessed thermodynamically by several physicochemical parameters such as O-H bond dissociation enthalpy (O-H_{BDE}), proton dissociation enthalpy (PDE), proton affinity (PA), ionization potential (IP) and electron transfer enthalpy (ETE).

As can be seen in **Figure 1**, the structural features of drometrizole (pi-conjugation, presence of hydroxyl group) and its above-mentioned properties warrant it to be a potent antioxidant-UV filter. Such a study is conveniently achieved via the use of density functional theory (DFT) and time-dependent DFT (TD-DFT) methods. DFT has been utilized by several authors to predict the relationship between the structure-activity of a compound and also for the design of novel potential antioxidants [17].

Within the framework of the design of more UV filter-antioxidant-based molecules, this work had as the main objective, to evaluate the thermodynamics of the antioxidant mechanism and UV-absorption properties of PBT using the DFT and TD-DFT methods. In addition, the effects of an electron-donating substituent (EDS) and an electron-accepting substituent (EAS) (see **Figure 1**) on the antioxidant activity and UV spectra of PBT were assessed. The effects of these substituents were explored with the intention of improving their anti-oxidant efficiencies. A comprehension of why a mechanism is favored over another requires in due course some kinetic studies to confirm speculations drawn from thermodynamic studies. However, this is not the main aim of this study. Here, we set out to specifically: 1) Find drometrizole derivatives with high antioxidant activity from a theoretical point of view; 2) Identify the substituent that are the most effective in reducing the BDE, IP, and PA; 3) Find the preferred mechanisms in the gas and solvent phases from a thermodynamic perspective; 4) Compute the UV spectra of these molecules. To achieve these, the physiochemical descriptors including O-H_{BDE}, IP, PDE, PA and ETE were computed to examine the HAT, SET-PT and SPLET mechanisms. Also, the frontier molecular orbitals (FMO) and energies of the studied molecules were computed. Furthermore, the transi-

tion wavelengths λ (nm), oscillator strengths (f), the major components of the molecular orbital (MO) transitions and configuration interaction (CI) were computed to elucidate the UV filtering ability of the investigated compounds. This study will serve as a base to create an awareness of the photoprotective properties of the compounds studied possible design and applications as sunscreen products.

2. Computational Details

All calculations in this study were done with the ORCA 4.2.1 program suite [18] [19]. Initial guess geometries were conceived by means of the Avogadro 1.2.1 visualization program [20]. For all reported calculations, a tight self-consistent field (SCF) criterion was utilized with a grid6 sized numerical quadrature. The restricted Kohn-Sham (RKS) formalism and its unrestricted counterpart (UKS) were adopted for closed and open-shell molecules (*i.e.* for radicals and radical cation species) respectively. The geometry of each drometrizole molecule (ArOH), their corresponding radicals ($ArO^{\bullet}$), cationic radicals ($ArOH^{\bullet+}$) and anions (ArO^{-}) were optimized in the gas phase with no constraints, using the low-cost B97-3c method. This method was used thanks to its efficient performance in geometry optimization and frequency calculations of organic, inorganic, and organo-metallic systems [21]. Only real frequencies were obtained from vibrational frequency calculations at the same level of theory as that used for geometry optimization, confirming the optimized geometries are minima on their potential energy surfaces. In all cases, no spin contamination was found.

The electronic energies from the B97-3c method were enhanced via single-point (SP) computations at a higher level of theory using the Minnesota exchange-correlation (XC) functional, M06-2X [22], together with the 6-311++G(d,p) basis set. The M06-2X functional was used owing to its reliability in calculating thermodynamic parameters [22]. The D3 dispersion correction with zero damping (D3Zero) was employed to justify long-range dispersion interactions in all SP calculations with the M06-2X functional. The resolution-of-identity (RI-J) approximation [23] and the Chain-of-Spheres (COSX) approximation [24], establishing the RIJCOSX approximation, were utilized with the suitable auxiliary basis sets to fasten the SP computations. Remarkably, the loss of accuracy from applying the RIJCOSX approximation is insignificant [25]. Reaction enthalpies were computed M06-2X/6-311++G(d,p) level of theory, by making use of the electronic energies obtained at this level with vibrational frequencies obtained from the B97-3c method, with the aid of the Kisthelp software.

To include solvent effects on the computed properties, a continuum solvation method termed Solvation Model Density (SMD) was employed [26] via SP calculations on the gas-phase optimized B97-3c geometries. SMD was used owing to its universal and applicable nature for any charged or uncharged solutes, with relatively low errors [27]. Water (dielectric constants, $\varepsilon = 78.35$) was used to mimic the aqueous environment.

Frontier molecular orbital energies of the studied molecules were obtained from the SP calculations. The HOMO-LUMO energy gaps (ΔE) of the studied compound were calculated based on the energies of the highest and lowest occupied molecular orbitals (E_{HOMO} and E_{LUMO}, respectively) as follows:

$$\Delta E = E_{\mathrm{LUMO}} - E_{\mathrm{HOMO}} \tag{1}$$

To compute the absorption spectra of the studied compounds, vertical electronic excitations from the minima of the ground-state structures were computed using the PBE0 functional [28] with the def2-TZVP Ahlrichs triple-ζ basis set [29], employing the time-dependent density functional theory (TD-DFT) as implemented in the ORCA software. PBE0 has been utilized because it produces computed values which corroborate their experimental counterparts [1]. The def2-TZVP basis set was employed since it is appropriate to compute electronic properties [29]. To account for long-range dispersion interactions, the Grimme's atom-pairwise dispersion correction with Becke-Johnson damping (D3BJ) [30] was employed. Using the TD-DFT method, electronic absorption properties (like the transition wavelengths λ (nm), oscillator strengths (f), the major components of the molecular orbital (MO) transitions and configuration interaction (CI)) of the studied compounds on the basis of the B97-3c optimized ground state geometries were obtained.

2.1. Antioxidant Potential

As stated before now the antioxidant capacity of phenolic compounds has been elucidated through several mechanisms. The commonly used ones are hydrogen atom transfer (HAT), single electron transfer followed by proton transfer (SET-PT), and sequential proton loss electron transfer (SPLET) [31]. These mechanisms individually offer an approach on how these molecules respond in the presence of a radical [15] [32]. It is worth noting that the previously mentioned mechanisms are liable to happen in parallel, however, at different rates. The above-mentioned mechanisms are presented in **Figure 2** and have been briefly discussed below.

2.1.1. Hydrogen Atom Transfer (HAT) Mechanism

This mechanism is characterized by the capacity of a free radical ($R^{\bullet}$) to remove a hydrogen atom from the antioxidant (ArOH), yielding the radical form of phenolic antioxidant ($ArO^{\bullet}$).

$$\mathrm{ArOH} \rightarrow \mathrm{ArO}^{\bullet} + \mathrm{H}^{\bullet} \tag{2}$$

2.1.2. Single Electron Transfer-Proton Transfer (SET-PT) Mechanism

The SET-PT mechanism is a two-step reaction. The first step is ruled by the ability of an antioxidant to transfer an electron, giving rise to a cationic radical ($ArOH^{\bullet+}$).

$$\mathrm{ArOH} \rightarrow \mathrm{ArOH}^{\bullet+} + \mathrm{e}^{-} \tag{3}$$

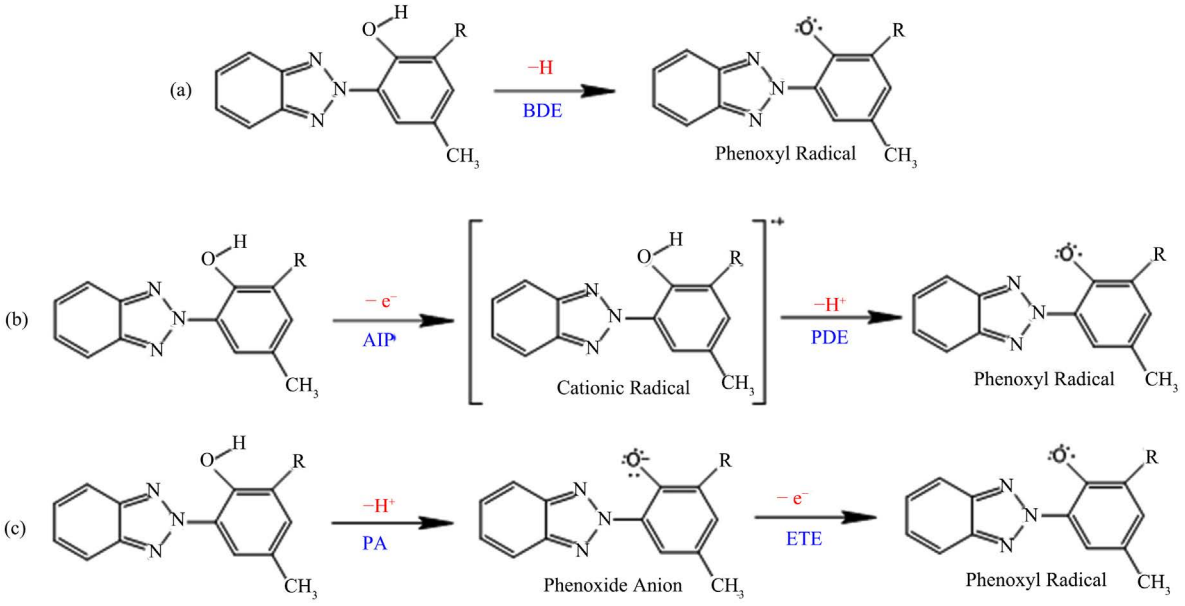

Figure 2. (a) HAT, (b) SET-PT and (c) SPLET mechanisms of the studied compounds.

In the second step, the $ArOH^{\bullet+}$ previously formed is deprotonated into a phenolic radical ($ArO^{\bullet}$).

$$ArOH^{\bullet+} \rightarrow ArO^{\bullet} + H^{+} \quad (4)$$

The numerical descriptors resulting from this mechanism are IP and PDE for the first and second reactions respectively.

2.2. Sequential Proton Loss Electron Transfer (SPLET) Mechanism

Like the SET-PT mechanism, the SPLET mechanism also consists of a two-step reaction. The first step corresponds to the deprotonation of the phenolic antioxidant, yielding the antioxidant anion (ArO^{-}).

$$ArOH \rightarrow ArO^{-} + H^{+} \quad (5)$$

The second step corresponds to the transfer of an electron form ArO^{-}, resulting in the formation of the phenoxyl radical ($ArO^{\bullet}$) of the antioxidant.

$$ArO^{-} \rightarrow ArO^{\bullet} + e^{-} \quad (6)$$

The numerical descriptors resulting from this mechanism are PA and ETE for the first and second steps respectively.

To investigate the likelihood of these mechanisms to occur, related thermodynamic parameters comprising: O-H bond dissociation enthalpy ($O\text{-}H_{BDE}$), ionization potential (IP), proton dissociation enthalpy (PDE), proton affinity (PA), and the electron transfer enthalpy (ETE) were assessed according to Equations (7-8) as:

$$BDE = H\left(BTO^{\bullet}\right) + H\left(H^{\bullet}\right) - H\left(BTOH\right) \quad (7)$$

$$IP = H\left(BTOH^{\bullet+}\right) + H\left(e^{-}\right) - H\left(BTOH\right) \quad (8)$$

$$PDE = H\left(BTO^{\bullet}\right) + H\left(H^{+}\right) - H\left(BTOH^{\bullet+}\right) \quad (9)$$

$$PA = H\left(BTO^{-}\right) + H\left(H^{+}\right) - H\left(BTOH\right) \quad (10)$$

$$ETE = H\left(BTO^{\bullet}\right) + H\left(e^{-}\right) - H\left(BTO^{-}\right) \quad (11)$$

where $H(BTOH)$, $H\left(BTO^{\bullet}\right)$, $H\left(H^{\bullet}\right)$, $H\left(BTOH^{\bullet+}\right)$, $H\left(BTO^{-}\right)$, $H\left(e^{-}\right)$, and $H\left(H^{+}\right)$ are enthalpies of the neutral molecule (antioxidant), neutral radical, hydrogen atom, radical cation, anion, electron, and proton, respectively. The gas phase $H\left(e^{-}\right)$, and $H\left(H^{+}\right)$ values for this study were obtained from [33] [34] [35], while those of $H\left(e^{-}\right)$, and $H\left(H^{+}\right)$ in the aqueous phase from [32]. The $H\left(H^{\bullet}\right)$ in the gaseous and aqueous phases for this study were computed at the M06-2x/6-311++G(d,P) level of theory.

3. Results and Discussion

3.1. Investigating the Suitability of the Optimized Structures

In order to assess the suitability of the B97-3c method and the accuracy of the optimized structures, a selection of gas-phase calculated bond lengths and angles of PBT have been likened to the corresponding experimental values obtained elsewhere [36]. The computed bond lengths and angles of PBT are enumerated in **Table S1** of the electronic **Supplementary Information** (ESI), alongside their corresponding experimental values. It can be perceived from **Table S1** that the theoretical bond lengths and angles agree with experimental data, indicating the suitability of the method used. For better comparison of these values, Pearson's linear regression was performed. Correlation coefficients (R^2) of 0.99 and 0.93 were found for the bond angles and bond lengths respectively. From the high R^2 values (very close to unity), the calculated bond lengths and bond angles of PBT agree perfectly with the experimental values, indicating the reliability of the optimized structures.

3.2. Geometrical Analyses

The fully optimized B97-3c geometries of the neutral forms of PBT, PBT1 and PBT2 in the gaseous phase are shown in **Figure 3**. Those of the corresponding radical, cationic radical and anionic forms are included in the accompanying ESI as visualized with the ChemCraft v1.7 software [37]. The Cartesian coordinates for all these structures are provided in the ESI. Selected geometric parameters of these molecules are listed in **Table 1** (see **Figure 1** for atom numbering). The selected parameters presented in **Table 1** originate from the 4-methoxy phenolic ring, as changes caused by the ED and EASs at the ortho position (C17 atom) of this ring, may yield some loss of planarity of PBT. As can be observed from the values presented in **Table 1** it is obvious that the type of substituents (*i.e.* EDS and EASs) on C17 of the 4-methoxy phenolic ring does not have a significant effect on the selected geometrical parameters. Also, it is inferred from the bond

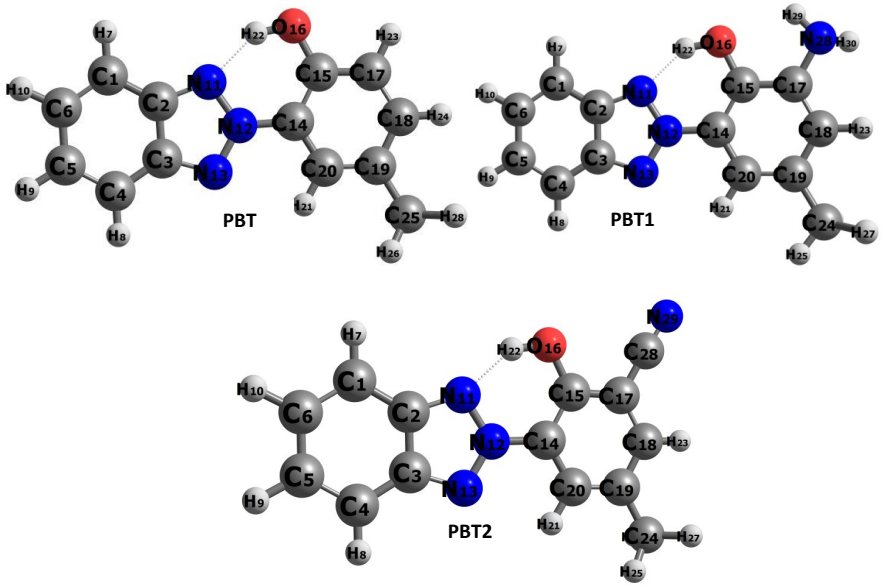

Figure 3. Optimized structures of the studied compounds obtained from B97-3c calculations in gas phase.

Table 1. Selected geometric parameters of PBT and ortho-substituted optimized with the B97-3C method gaseous phase.

Parameters	PBT	PBT1	PBT2
	Bond lengths (Å)		
N11-N12	1.341	1.342	1.341
N12-N13	1.326	1.325	1.325
C14-C15	1.408	1.399	1.408
C15-O16	1.343	1.351	1.333
C15-C17	1.396	1.410	1.409
C17-C18	1.377	1.386	1.393
C18-C19	1.398	1.396	1.389
C19-C20	1.382	1.380	1.386
	Bond angles (˚)		
N11-N12-N13	116.3	116.2	116.4
C14-C15-C17	117.4	118.5	117.1
C15-C17-C18	121.3	119.0	120.9
C17-C18-C19	121.5	122.0	121.5
C18-C19-C20	117.8	118.9	117.9
O16-C15-C17	118.0	116.4	118.2
	Dihedral angles (˚)		
O16-C15-C14-C20	−179.8	179.5	−179.8
O16-C15-C17-C18	179.8	−179.4	179.8
C14-C15-C17-C18	0.1	−0.2	0.1
C14-C20-C19-C18	0.2	0.4	0.3

length values listed in Table 1 that for each molecule investigated, the numerical values are close to 120˚, suggesting that the atoms in the 4-methoxy phenol ring are nearly sp^2 hybridized and are therefore very likely to adopt a highly planar arrangement. That notwithstanding, the planarity of these molecules is likely to be significantly reduced owing to free-rotation around the N12-C14 bond. Nevertheless, the rotation is highly hindered by the intramolecular hydrogen bonds O16-H22···N11 which also stabilize the molecules. Also, from the torsional angles in the 4-methoxy phenolic ring listed in Table 1 are close to 0˚ or 180˚. On the basis of the ongoing, the optimized molecular geometries of the studied molecules are highly planar and there is no significant effect with the presence of the EDS and EASs.

3.3. Antioxidant Properties of the Studied Molecules

In this study, the relative values are referred to those of phenol, generally designated as the zero compound [38].

3.3.1. Evaluation of the HAT Mechanism

As earlier mentioned, O-H_{BDE} is the numerical parameter related to the HAT mechanism. It characterizes the stability of the corresponding hydroxyl group. Lower O-H_{BDE} values designate lower stability and the ease to which the equivalent O-H bond is broken, giving rise to a higher antioxidant activity [39]. The O-H_{BDE} values of the studied molecules were calculated from Equation (2) and the results are presented in Table 2 in the gas and aqueous phases. As can be seen from Table 2, the O-H_{BDE} values of the molecules under study are larger in the gaseous phase (by about 21 kJ/mol), implying that H-atom abstraction is more difficult in the gaseous phase.

It is also found in Table 2 that the difference between the O-H_{BDE} values of PBT and that PBT1 is approximately 42 and 46 kJ/mol, while that with PBT2 is about −6 and −9 kJ/mol in the gas and aqueous phases respectively. This means that the presence of -NH2 lowers the O-H_{BDE} values, while that of -CN increases this value as compared to that of PBT. This variation is attributed to the fact

Table 2. Computed O-H bond dissociation energies (O-H_{BDE}) (in kJ/mol) of the studied compounds obtained at the M06-2x-D3(BJ)/6-311++G(d,p) level of theory.

	HAT	
Molecular species	Gas	Water
Phenol	372.2 (0.0)[a]	376.7 (0.0)
PBT	398.0 (25.9)	376.9 (0.2)
PBT1	356.1 (−16.0)	331.1 (−45.6)
PBT2	404.0 (31.9)	385.6 (8.9)

[a]Refer to phenol for the relative O-H_{BDE} values (in the parentheses).

that EASs in the ortho-position stabilize the parent molecule and destabilize the radical, causing a rise in the O-H_{BDE} values. Contrariwise, EDSs in ortho-position have an opposite effect, leading to a reduction in the O-H_{BDE} values. The O-H_{BDE} values of the studied compounds were compared to that of phenol at the same theoretical level, and it is observed that PBT1 has a lower value (by about 16 and 45 kJ/mol in both study environments respectively). This clearly shows that PBT1 has a better antioxidant potential than phenol. In all investigated media, the lowest O-H_{BDE} was recorded for PBT1, while the highest for PBT2. This implies that H-atom abstraction is easier in PBT1 and more difficult in PBT2. On the basis of the O-H_{BDE} and the HAT mechanism, the antioxidant activity decreases as follows: PBT1 > PBT > PBT2 in all studied medium.

Spin density distributions

The spin density distribution is a well-grounded parameter that offers a better illustration of the reactivity of a radical system. Lower spin density distribution values yield a higher delocalization of the spin density in a given radical. The computed spin densities on the oxygen atom of the phenoxy radicals (PBT, PBT1 and PBT2) in the gas and aqueous phases are presented in Table 3. Results from this table indicate that the spin density on the oxygen atom of the PBT1 radical is lower than those of the PBT and PBT2 radicals in both studied environments, implying that radical PBT1 has the highest stability and consequently is the least reactive in radical reactions. This result is allied to the lowest O-H_{BDE} values of PBT1 from Table 2, whereby PBT1 is the best antioxidant molecule.

3.3.2. Evaluation of the SET-PT Mechanism

As stated earlier, the ionization potential (IP) and proton dissociation enthalpy (PDE) are the descriptors associated with the two-step SET-PT mechanism. Molecules with low IP values are more susceptible to ionization and have potent antioxidant properties. The lower the IP value for a given molecule, the higher its electron donating ability and higher antioxidant activity [40]. For this study, the IP and PDE values of the molecules studied were computed from Equations (3) and (4) respectively and the values alongside that of phenol in the vacuum and aqueous phase are listed in Table 4. In this table, it is evident that the IP values of the compounds under study are less than that of phenol in both studied environments. Implying that the investigated molecules have a greater tendency to give out electrons than phenol and consequently have better antioxidant properties than the latter. From this table, the difference between the IP value of PBT

Table 3. Spin density values on the O-radical of the studied compounds computed at the at the M06-2x-D3(BJ)/6-311++G(d,p) level of theory.

Molecular species	Gas	Water
PBT	0.3936	0.3252
PBT1	0.3264	0.2609
PBT2	0.3699	0.3068

Table 4. Computed ionization potential (IP) and proton dissociation energies (PDE) (in kJ/mol) of the studied compounds obtained at the M06-2x-D3(BJ)/6-311++G(d,p) level of theory.

Molecular species	SET-PT			
	IP		PDE	
	Gas	Water	Gas	Water
Phenol	825.8 (0.0)[b]	521.0 (0.0)	857.5 (0.0)[c]	18.7 (0.0)
PBT	759.5 (−66.3)	509.4 (−11.60)	949.6 (92.1)	30.5 (11.8)
PBT1	693.7 (−132.1)	443.3 (−77.5)	973.6 (116.1)	50.9 (32.2)
PBT2	805.0 (−20.8)	539.4 (18.35)	910.2 (52.7)	9.3 (−9.4)

[b]Refer to phenol for the relative IP and PDE values (in the parentheses); [c]Refer to phenol for the relative PDE values (in the parentheses).

and PBT1 is 66 kJ/mol in both media while that of PBT and PBT2 are −45 and −30 kJ/mol in the gas and aqueous respectively. Clearly, from Table 4, the lowest IP value was found to be for PBT1 while the highest for PBT2 in all studied environments. This indicates that PBT1 has the greatest ability to donate electrons while the reverse is true for PBT2. Additionally, Table 4 shows that the presence of the EDS reduces the IP values, while that of the EAS increases this value as compared to that of PBT in both media. The increase in the IP values is attributed to the fact the EAS stabilizes the parent molecule and destabilizes $ArOH^{\bullet+}$, while the decrease in IP values is due to the fact that the EDS tends to stabilize $ArOH^{\bullet+}$ and destabilize the parent molecule.

Also, it can be seen in Table 4 that the formation of $ArOH^{\bullet+}$ for the molecules under investigation is easier in water (by about 255 kJ/mol). This indicates that the formed radical cation, $ArOH^{\bullet+}$ is more stable in water due to the delocalization of π-electrons. This result agrees with that in [40], which confirms that electron donation is easier in the solvent, particularly polar medium (water in this case). On the basis of the ongoing, the increasing IP trend is: PBT1 < PBT < PBT2.

PDE describes the potential of the cationic radical, $ArOH^{\bullet+}$ to transfer a proton to the free radical. Molecules with lower PDE values are more susceptible to proton loss [41]. As can be seen from Table 4, the highest PDE values are found for PBT1, whereas lowest for PBT2. This observation is as a result of the fact that the presence of the EDS in PBT1 stabilizes $ArOH^{\bullet+}$ but destabilizes the parent molecule, while the presence of the EAS in PBT2 have an opposite effect. These results are in accordance with a previous paper on substituted phenols [42]. From a thermodynamic view point, the first step (IP) is the most important. From the values reported in Table 4, the SET-PT mechanism is not preferred in the gas phase due to the fact that the IP and PDE values are higher than the corresponding aqueous phase values. The significant decrease in both parameters (predominantly the PDE values) in aqueous phase implies the ease in the proton transfer and electron abstraction processes respectively. This observation is sim-

ilar to that obtained in [31].

3.3.3. Evaluation of the SPLET Mechanism

As earlier mentioned, the proton affinity (PA) and electron transfer enthalpy (ETE) parameters are linked to the SPLET mechanism. The PA and ETE values of the compounds studied were calculated according to Equations (5) and (6) respectively in the gaseous and aqueous phases together with those of phenol are enumerated in Table 5. The proton loss (characterized by the PA values) is the underlying step in the SPLET mechanism. Lower PA values favor the deprotonation of the drometrizole antioxidants yielding the phenoxyl anion. It can be seen from Table 5 that the PA values for all studied compounds are higher in the gaseous phase than in the aqueous phase, suggesting that the proton loss is highly preferred in aqueous phase. In addition, it can be inferred from Table 5 that the PA values of the molecules under investigation are lower than those of phenol.

Electron transfer (characterized by the ETE values) from the phenoxide ion represents the second step in SPLET mechanism. ETE denotes the capacity of the antioxidant anion to transfer electrons to the free radical. The lower the ETE value for a given molecule, the more active is the resulting phenoxide anion. From Table 5, the ETE values in the gas and aqueous phases follow the same sequence: $ETE_{PBT1} < ETE_{PBT} < ETE_{PBT2}$. In aqueous media, the ETE values of the studied compounds are higher than the PA values but enough to account for the second step of SPLET mechanism. It is evident from Table 5 that the lowest ETE value corresponds to PBT1 while the highest to PBT2 in all studied environments. This shows that PBT1 has a greater tendency to transfer electrons to the free radical and the ease with which it forms the corresponding phenoxide anion, while the reverse is the case for PBT2. Also, it is obvious from Table 5 that the presence of the EDS in PBT1 decreases the ETE value, while that of the EAS in PBT2 increases this value as compared to PBT. It can also be seen in Table 5 that the formation of the phenoxide anion for the investigated molecules is easier in the aqueous phase than in the gaseous phase. On the basis of the ETE values, PBT1 is the best anti-oxidant molecule, while PBT2 is the least.

Table 5. Computed proton affinities (PA) and electron transfer energies (ETE) (in kJ/mol) of the studied compounds obtained at the M06-2x-D3(BJ)/6-311++G(d,p) level of theory.

Molecular species	SPLET			
	PA		ETE	
	Gas	Water	Gas	Water
Phenol	1453.1 (0.0)[d]	152.3 (0.0)	230.2 (0.0)[e]	387.5 (0.0)
PBT	1439.1 (−14)	149.9 (−2.4)	270.0 (39.8)	390.1 (2.6)
PBT1	1432.6 (−20.5)	152.9 (0.6)	234.7 (4.5)	341.3 (−46.2)
PBT2	1379.3 (−73.8)	118.5 (−33.8)	335.9 (105.7)	430.2 (42.7)

[d]Refer to phenol for the relative PA values (in the parentheses); [e]Refer to phenol for the relative ETE values (in the parentheses)

To ease comparisons, the O-H_{BDE}, IP and PA values for all the molecules investigated were plotted on the same axes and are presented on Figure 4(a) and Figure 4(b) for the gas and aqueous phases respectively. It is obvious from Figure 4(a) that the computed PA values of the studied molecules are higher than the equivalent IP and O-H_{BDE} values. This illustrates that in the gas phase, the favored mechanism can be classified thermodynamically as: HAT < SET-PT < SPLET. In the same manner, it can be seen from Figure 4(b) that the PA values of the compounds investigated are remarkably lower than the corresponding O-HBDE and IP values. Therefore, in aqueous phase, the SPLET mechanism represents the most probable reaction pathway from thermodynamic point of view. In the aqueous phase, the trend is: SPLET < SET-PT < HAT. This trend ascertains the importance of this mechanism in a polar solvent as reported elsewhere [43]. Conclusively, among the three mechanisms investigated, the HAT mechanism is thermodynamically favored in the gas phase and SPLET in water.

3.4. Frontier Molecular Orbital (FMO) Analyses

FMOs are important parameters which portray electronic properties as well as reactivity of a molecule. The Highest Occupied Molecular Orbital (HOMO) and Lowest Unoccupied Molecular Orbital (LUMO) distribution can equally be utilized to describe the antioxidant capabilities of a molecule [44]. Knowledge of the HOMO distribution can be used to deduce the probable site for attack by free radicals in the molecule.

As can be seen from Table 6, the HOMO of PBT1 is mainly localized on the 4-methylphenolic moiety, while those PBT and PBT2, are appreciably distributed over their entire molecular structures (*i.e.* on the 4-methylphenolic and benzotriazole moieties). This suggests the probable sites for radical attack.

On the basis of FMO and the Fukui theories, FMO energies (*i.e.* E_{HOMO}, and E_{LUMO} are vital to predict chemical reactivity and stability of molecules. The E_{HOMO}

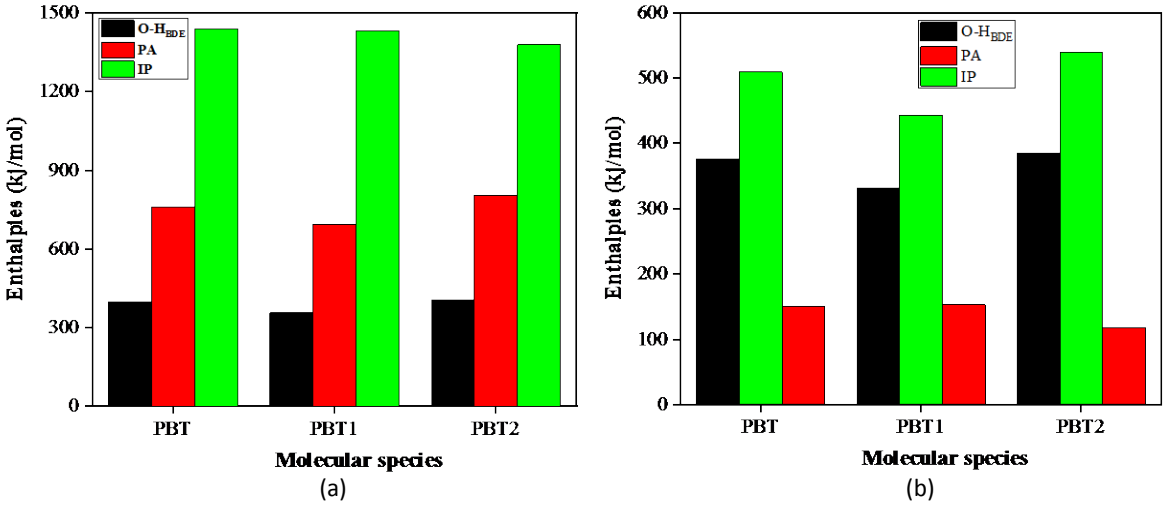

Figure 4. Plot of enthalpy values (kJ/mol) with molecular species in (a) Gas and (b) Aqueous phases computed at the M06-2x-Zero/6-311++G(d,p) level of theory in gas and aqueous phases.

Table 6. HOMO distributions of the studied molecules obtained at the M062x-D3Zero/6-311++G(d,p) level of theory.

Species	Gas phase	Aqueous phase
PBT	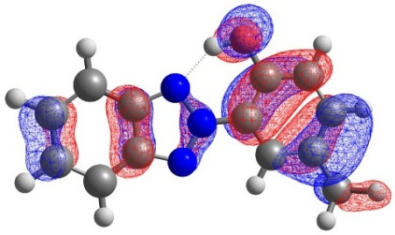	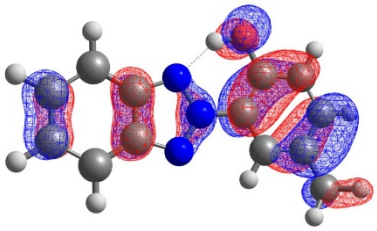
PBT1	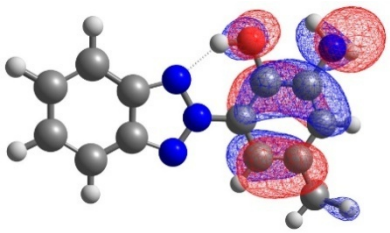	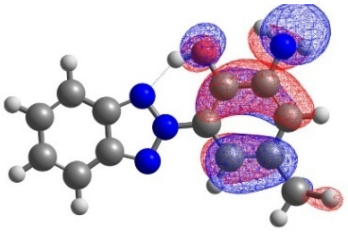
PBT2	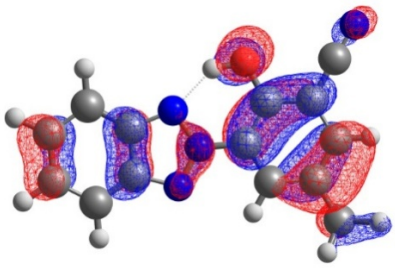	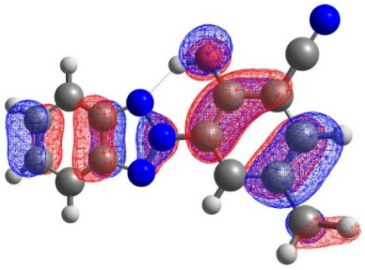

is another parameter to measure the electron-donating ability of antioxidants. The higher the E_{HOMO} value, the greater the tendency of a molecule to donate electrons is and consequently a higher antioxidant is potential. The HOMO-LUMO energy gap, ΔE in turn provides information on the chemical activity of the molecule. The computed E_{HOMO}, E_{LUMO} and ΔE values of the studied molecules in the gas and aqueous phases are summarized in Table 7.

It can be seen in Table 7 that the presence of the EDS (-NH_2) in PBT1 increases E_{HOMO} (*i.e.* it becomes less negative), while the presence of EAS (-CN) in PBT2 reduces E_{HOMO} (*i.e.* it becomes more negative) as compared to that of PBT. Consequently, drometrizoles with strong EDSs are better electron-donors, *i.e.*, they easily partake in the SET-PT mechanism than those with EASs. Accordingly, the electron-donating ability of the studied molecules increases in the order: PBT2 < PBT < PBT1. From its relatively high E_{HOMO} values, PBT1 is the most chemically reactive species among the molecules studied. This is attributable to the presence of the -NH2 group at the ortho-position of the -OH group, which acts as an EDS by means of its positive inductive (+I) effect which activates the 4-methoxy phenolic ring, making it more reactive. The IP trend is consistent with the data presented in Table 7, confirming that PBT1 is the best electron-donor among the investigated compounds. From this trend, we conclude that

Table 7. Calculated E_{HOMO}, E_{LUMO} and ΔE (eV) of drometrizole and its ortho-substituted derivatives computed at the M06-2x-D3(BJ)/6-311++G(d,p) level of theory in gas and aqueous phases.

Molecular species		Gas			Aqueous		
Substituents	Notations	E_{HOMO}	E_{LUMO}	ΔE	E_{HOMO}	E_{LUMO}	ΔE
-H	PBT	−7.3891	−1.4268	5.9623	−7.4763	−1.4161	6.0602
-NH_2	PBT1	−6.9245	−1.3510	5.5735	−7.0732	−1.3879	5.6853
-CN	PBT2	−7.9124	−1.8554	6.0570	−7.7558	−1.6143	6.1415

E_{HOMO} can be rapidly used to estimate the reaction enthalpies of the first step of the SET-PT mechanism. These dependences can be used to select appropriate substituents for the synthesis of novel drometrizole-based derivatives with improved antioxidant activity [45].

ΔE provides valuable information on the reactivity and stability of molecules [46] [47]. The ΔE values of species investigated in this work were calculated according to Equation (1). It is obvious from the values reported in **Table 7** that PBT1 has the lowest ΔE values while PBT2 has the highest. Accordingly, the transfer of electrons from HOMO to LUMO in PBT1 is relatively easier than in the other studied compounds. Based on the ΔE values of the studied compounds, the order of decreasing ΔE is: $\Delta E_{PBT2} > \Delta E_{PBT} > \Delta E_{PBT1}$. This trend is consistent with those obtained from the E_{HOMO} values. PBT1 was predicted to be the most reactive and consequently, has the best antioxidant activity amongst the studied molecules. This result is in perfect agreement with the predicted antioxidant activity as presented in **Table 3**.

3.5. Computed Electronic Absorption Spectra of the Studied Compounds

To assess the ability of PBT to screen UV radiations and the effect of ED and EASs, their electronic absorption spectra were simulated at the TD-DFT/PBE0-D3(BJ)/def2-TZVP levels of theory in gas and aqueous (water solvent) phases. The spectral data obtained is presented in **Table 8**. Listed in **Table 8** are the vertical absorption transition wavelengths (λabs in nm), the oscillator strengths (f), the configuration interaction (CI) or molecular orbital percentage contributions, and the prominent electronic transitions. As can be seen in **Table 8**, two absorption bands with the maximum band centered around 334, and the shoulder band around 282 nm are observed in the absorption spectrum of PBT in both the gas and water solvent. These bands correspond to S0→S1 and S0→S2 transitions respectively. Interestingly, these values are very close to the experimentally obtained absorption spectrum of PBT obtained in [1], which shows two intense bands centered around 330 and 280 nm. This result confirms the suitability of the level of theory used. The relatively high oscillator strengths of the calculated electronic transitions indicate their high intensities. The observed transitions: S0→S1, and S0→S2 originate from the molecular orbitals: HOMO (H), HOMO-2 (H-2)

Table 8. Transition wavelengths λ (nm), oscillator strengths (f), the major components of the molecular orbital (MO) transitions and configuration interaction (CI) for PBT and derivatives computed at PBE0-D3(BJ)/def2-TZVP level of theory.

Species	Media	Transition	λabs (nm)	f	MO contribution	CI (%)
PBT	Gas	S0→S1	340	0.3587	H→L	96.42
		S0→S2	283	0.4250	H-2→L	76.78
	Water	S0→S1	333	0.3713	H→L	95.88
		S0→S2	284	0.1431	H-1→L	88.87
PBT1	Gas	S0→S1	395	0.0411	H→L	98.54
		S0→S2	313	0.7123	H-1→L	97.71
	Water	S0→S1	387	0.0367	H→L	98.52
		S0→S2	310	0.7145	H-1→L	97.67
PBT2	Gas	S0→S1	336	0.4074	H→L	95.72
		S0→S2	288	0.0676	H-1→L	94.36
	Water	S0→S1	327	0.4735	H→L	94.92
		S0→S2	294	0.0331	H-1→L	96.28

and HOMO-1 (H-1), respectively, and terminate in the molecular orbital LUMO (L) in each case. In the gas phase, the maximum absorption is due to the transition from H→L and the shoulder peak due to transitions from H-2→L. In water, the maximum absorption is due to the transition from H→L and the shoulder peak due to the H-1→L transitions. It is evident from the results obtained that PBT has an absorption in the region 283 - 340 nm, and can effectively absorb the dangerous UV A and UV B radiations from sunlight. This result is in accordance with that obtained elsewhere [1].

Further search for enhanced UV filter molecules based on the drometrizole moiety led to the absorption spectra of the designed drometrizole derivatives studied and the results are presented in Table 8.

From this table, two intense absorption bands with the maximum band centered around 361, and the shoulder band around 301 nm in both the gas and water solvent are visible. These bands like those for PBT correspond to the S0→S1 and S0→S2 transitions respectively. These transitions correspond to the H→L and H-1→L for the maximum absorption and the shoulder peak respectively in both environments studied. It is also observed from Table 8 that all the absorption bands are red shifted as compared to that of PBT by factors of 33 and 21 nm for the maximum absorption and the shoulder peaks respectively in both environments under study. This bathochromic shift results from the presence of the EDS ($-NH_2$) at the ortho-position of the -OH group on the drometrizole moiety *i.e.* corresponding to PBT1. No significant change is observed for the molecules obtained from substitutions at the ortho-position with the presence of the EAS (-CN) *i.e.* the PBT2 molecule. It is important to point out that the derivatives of PBT have absorptions in the region 288 - 395 nm, implying that they can readily

absorb the hazardous UV A and UV B radiations from sunlight.

On the basis of the ongoing, the studied compounds especially PBT1 are potential candidates for the manufacture of UV filters and sunscreen lotions to fight the devastating effects of UV A and UVB radiations.

4. Conclusion

The antioxidant and UV spectral characteristics of Drometrizole (PBT) and the effect of an electron-donating group (ED), $-NH_2$ and an electron-attracting group (EA), -CN groups on these properties have been analyzed theoretically in the gas and aqueous phases. From a thermodynamic perspective, the HAT mechanism is preferred in the gas phase, while SPLET in the aqueous phase. Also, it is observed that the presence of $-NH_2$ reduces the $O\text{-}H_{BDE}$ and IP values, while that of -CN increases the PA values. Consequently, the molecule with the ED substituent (PBT1) is identified to be the compound with the highest antioxidant activity among the studied molecules. The spin density values on the O-radical are the lowest for PBT1 confirming that it is the best antioxidant molecule. The UV spectra of these molecules exhibit two intense absorption bands within the 280 - 400 nm region. This corresponds to the UV A and UV B regions of the electromagnetic spectrum. The major transitions in the UV-Visible spectra of the studied compounds are between the HOMO, HOMO-1 and HOMO-2 with LUMO level. The presence of the ED substituent is found to cause a bathochromic shift in absorption wavelengths. The studied molecules especially PBT1 can thus be considered as a potent antioxidant and UV absorption agent. The antioxidant capability of these molecules is therefore an added advantage for photoprotection as they can scavenge the free radicals. Results from this study can further be used for the design and synthesis of compounds with more improved photoprotective properties for applications in sunscreen products. Also, this study gives way for a subsequent kinetic study to make perfect the results deduced from this thermodynamic study.

Acknowledgements

We gratefully acknowledge the annual research modernization grant to lecturers by the Ministry of Higher Education of Cameroon.

Conflicts of Interest

The authors declare no conflicts of interest regarding the publication of this paper.

References

[1] Tasheh, N.S., Nkungli, N.K. and Ghogomu, J.N. (2019) A DFT and TD-DFT Study of ESIPT-Mediated NLO Switching and UV Absorption by 2-(2'-hydroxy-5'-methylphenyl) Benzotriazole. *Theoretical Chemistry Accounts*, **138**, Article No. 100. https://doi.org/10.1007/s00214-019-2488-0

[2] Dunaway, S., Odin, R., Zhou, L., Ji, L., Zhang, Y. and Kadekaro, A.L. (2018) Natural

Antioxidants: Multiple Mechanisms to Protect Skin from Solar Radiation. *Frontiers in pharmacology*, **9**, Article No. 392. https://doi.org/10.3389/fphar.2018.00392

[3] Chinh, N.T., Le Anh, N.T., Thao, P.T. and Quang, D.D. (2020) Photoprotective Properties of Natural Antioxidant Flavonoids: A DFT and TD-DFT Study on Acridone Derivatives. *Vietnam Journal of Chemistry*, **58**, 157-161. https://doi.org/10.1002/vjch.201900083

[4] Dao, D.Q., Phan, T. T. T., Nguyen, T.L.A., Trinh, P.T. H., Tran, T.T.V., Lee, J.S., *et al.* (2020) Insight into Antioxidant and Photoprotective Properties of Natural Compounds from Marine Fungus. *Journal of Chemical Information and Modeling*, **60**, 1329-1351. https://doi.org/10.1021/acs.jcim.9b00964

[5] Abiola, T.T., Rodrigues, N.D.N., Ho, C., Coxon, D.J., Horbury, M.D., Toldo, J.M., *et al.* (2020) New Generation UV-A Filters: Understanding their Photodynamics on a Human Skin Mimic. *The Journal of Physical Chemistry Letters*, **12**, 337-344. https://doi.org/10.1021/acs.jpclett.0c03004

[6] Shireen, P.A., Mujeeb, V.A. and Muraleedharan, K. (2017) Theoretical Insights on Flavanones as Antioxidants and UV Filters: A TDDFT and NLMO Study. *Journal of Photochemistry and Photobiology B*: *Biology*, **170**, 286-294. https://doi.org/10.1016/j.jphotobiol.2017.04.021

[7] Galanakis, C.M., Tsatalas, P. and Galanakis, I.M. (2018) Phenols from Olive Mill Wastewater and Other Natural Antioxidants as UV Filters in Sunscreens. *Environmental Technology & Innovation*, **9**, 160-168. https://doi.org/10.1016/j.eti.2017.12.002

[8] Lorigo, M. and Cairrao, E. (2019) Antioxidants as Stabilizers of UV Filters: An Example for the UV-B Filter Octylmethoxycinnamate. *Biomedical Dermatology*, **3**, Article No. 11. https://doi.org/10.1186/s41702-019-0048-9

[9] Rajan, V.K., Ahamed, T.S. and Muraleedharan, K. (2018) Studies on the UV Filtering and Radical Scavenging Capacity of the Bitter Masking Flavanone Eriodictyol. *Journal of Photochemistry and Photobiology B*: *Biology*, **185**, 254-261. https://doi.org/10.1016/j.jphotobiol.2018.06.017

[10] Liu, T. and Wu, D. (2011) Simultaneous Determination of Some Ultraviolet-Absorbing Chemicals in Sunscreen Cosmetics Using a High-Performance Liquid Chromatography Method. *International Journal of Cosmetic Science*, **33**, 408-415. https://doi.org/10.1111/j.1468-2494.2011.00643.x

[11] El-Asmy, H.A., Butler, I.S., Mouhri, Z.S., Jean-Claude, B.J., Emmam, M.S. and Mostafa, S.I. (2014) Zinc (II), Ruthenium (II), Rhodium (III), Palladium (II), Silver (I), Platinum (II) and MoO_2^{2+} Complexes of 2-(2'-hydroxy-5'-methylphenyl)-benzotriazole as Simple or Primary Ligand and 2, 2'-bipyridyl, 9, 10-phenanthroline or Triphenylphosphine as Secondary Ligands: Structure and Anticancer Activity. *Journal of Molecular Structure*, **1059**, 193-201. https://doi.org/10.1016/j.molstruc.2013.11.039

[12] Lee, J.K., Kim, K.B., Lee, J.D., Shin, C.Y., Kwack, S.J., Lee, B.M. and Lee, J.Y. (2019) Risk Assessment of Drometrizole, a Cosmetic Ingredient Used as an Ultraviolet Light Absorber. *Toxicological Research*, **35**, 119-129. https://doi.org/10.5487/TR.2019.35.2.119

[13] Lee, C.Y., Sharma, A., Semenya, J., Anamoah, C., Chapman, K.N. and Barone, V. (2020) Computational Study of *Ortho*-Substituent Effects on Antioxidant Activities of Phenolic Dendritic Antioxidants. *Antioxidants*, **9**, Article No. 189. https://doi.org/10.3390/antiox9030189

[14] Javan, A.J., Javan, M.J. and Tehrani, Z.A. (2013) Theoretical Investigation on Anti-

oxidant Activity of Bromophenols from the Marine Red Alga *Rhodomela confervoides*: H-Atom vs Electron Transfer Mechanism. *Journal of agricultural and food chemistry*, **61**, 1534-1541. https://doi.org/10.1021/jf304926m

[15] Galano, A., Mazzone, G., Alvarez-Diduk, R., Marino, T., Alvarez-Idaboy, J.R. and Russo, N. (2016) Food Antioxidants: Chemical Insights at the Molecular Level. *Annual Review of Food Science and Technology*, **7**, 335-352. https://doi.org/10.1146/annurev-food-041715-033206

[16] Vo, Q.V., Nam, P.C., Van Bay, M., Thong, N.M., Cuong, N.D. and Mechler, A. (2018) Density Functional Theory Study of the Role of Benzylic Hydrogen Atoms in the Antioxidant Properties of Lignans. *Scientific Reports*, **8**, Article No. 12361. https://doi.org/10.1038/s41598-018-30860-5

[17] Wang, G., Liu, Y., Zhang, L., An, L., Chen, R., Liu, Y., *et al.* (2020) Computational Study on the Antioxidant Property of Coumarin-Fused Coumarins. *Food Chemistry*, **304**, Article ID: 125446. https://doi.org/10.1016/j.foodchem.2019.125446

[18] Neese, F. (2012) The ORCA Program System. *WIREs Computational Molecular Science*, **2**, 73-78. https://doi.org/10.1002/wcms.81

[19] Neese, F. (2017) Software Update: The ORCA Program System, Version 4.0. *WIREs Computational Molecular Science*, **8**, e1327. https://doi.org/10.1002/wcms.1327

[20] Hanwell, M.D., Curtis, D.E., Lonie, D.C., Vandermeersch, T., Zurek, E. and Hutchison, G.R. (2012) Avogadro: An Advanced Semantic Chemical Editor, Visualization, and Analysis Platform. *Journal of Cheminformatics*, **4**, Article No. 17. https://doi.org/10.1186/1758-2946-4-17

[21] Brandenburg, J.G., Bannwarth, C., Hansen, A. and Grimme, S. (2018) B97-3c: A Revised Low-Cost Variant of the B97-D Density Functional Method. *The Journal of Chemical Physics*, **148**, Article ID: 064104. https://doi.org/10.1063/1.5012601

[22] Zhao, Y. and Truhlar, D.G. (2008) The M06 Suite of Density Functionals for Main Group Thermochemistry, Thermochemical Kinetics, Noncovalent Interactions, Excited States, and Transition Elements: Two New Functionals and Systematic Testing of Four M06-Class Functionals and 12 Other Functionals. *Theoretical Chemistry accounts*, **120**, 215-241. https://doi.org/10.1007/s00214-007-0310-x

[23] Neese, F., (2003) An Improvement of the Resolution of the Identity Approximation for the Formation of the Coulomb Matrix. *Journal of Computational Chemistry*, **24**, 1740-1747. https://doi.org/10.1002/jcc.10318

[24] Neese, F., Wennmohs, F., Hansen, A. and Becker, U. (2009) Efficient, Approximate and Parallel Hartree-Fock and hybrid DFT Calculations. A 'Chain-of-Spheres' Algorithm for the Hartree-Fock Exchange. *Chemical Physics*, **356**, 98-109. https://doi.org/10.1016/j.chemphys.2008.10.036

[25] Goerigk, L. and Grimme, S. (2011) A Thorough Benchmark of Density Functional Methods for General Main Group Thermochemistry, Kinetics, and Noncovalent Interactions. *Physical Chemistry Chemical Physics*, **13**, 6670-6688. https://doi.org/10.1039/C0CP02984J

[26] Marenich, A.V., Cramer, C.J. and Truhlar, D.G. (2009) Universal Solvation Model Based Onsolute Electron Density and on a Continuum Model of the Solvent Defined by the Bulk Dielectric Constant and Atomic Surface Tensions. *The Journal of Physical Chemistry B*, **113**, 6378-6396. https://doi.org/10.1021/jp810292n

[27] Bine, F.K., Tasheh, S.N. and Nkungli, N.K. (2020) Corrosion Inhibition of Aluminium in Gas and Acid Media by Some Chalcone-Based N-(3-Aminopropyl) Imidazoles: TD-DFT-Based FMO, Conceptual DFT, QTAIM and EDA Studies. *Computa-*

tional Chemistry, **9**, 37-63. https://doi.org/10.4236/cc.2021.91003

[28] Grimme, S., Brandenburg, J.G., Bannwarth, C. and Hansen, A. (2015) Consistent Structures and Interactions by Density Functional Theory with Small Atomic Orbital Basis Sets. *Journal of Chemical Physics*, **143**, Article ID: 054107. https://doi.org/10.1063/1.4927476

[29] Weigend, F. and Ahlrichs, R. (2005) Balanced Basis Sets of Split Valence, Triple Zeta Valence and Quadruple Zeta Valence Quality for H to Rn: Design and Assessment of Accuracy. *Physical Chemistry Chemical Physics*, **7**, 3297-3305. https://doi.org/10.1039/B508541A

[30] Caldeweyher, E., Bannwarth, C. and Grimme, S. (2017) Extension of the D3 Dispersion Coefficient Model. *The Journal of Chemical Physics*, **147**, Article ID: 034112. https://doi.org/10.1063/1.4993215

[31] Ahamed, T.S., Rajan, V.K., Sabira, K. and Muraleedharan, K. (2019) DFT and QTAIM Based Investigation on the Structure and Antioxidant Behavior of Lichen Substances Atranorin, Evernic acid and Diffractaic Acid. *Computational biology and chemistry*, **80**, 66-78. https://doi.org/10.1016/j.compbiolchem.2019.03.009

[32] Marković, Z., Marković, Z., Tošović, J., Milenković, D. and Marković, S. (2016) Revisiting the Solvation Enthalpies and Free Energies of the Proton and Electron in Various Solvents. *Computational and Theoretical Chemistry*, **1077**, 11-17. https://doi.org/10.1016/j.comptc.2015.09.007

[33] Bartmess, J.E. (1994) Thermodynamics of the Electron and the Proton. *The Journal of Physical Chemistry*, **98**, 6420-6424. https://doi.org/10.1021/j100076a029

[34] Bizarro, Cabral, B.C., Dos Santos, R.B. and Simões, J.M. (1999) Substituent Effects on the O-H Bond Dissociation Enthalpies in Phenolic Compounds: Agreements and Controversies. *Pure and Applied Chemistry*, **71**, 1249-1256. https://doi.org/10.1351/pac199971081609

[35] Boulebd, H. (2020) The Role of Benzylic-Allylic Hydrogen Atoms on the Antiradical Activity of Prenylated Natural Chalcones: A Thermodynamic and Kinetic Study. *Journal of Biomolecular Structure and Dynamics*, **39**, 1955-1964. https://doi.org/10.1080/07391102.2020.1740791

[36] Catalán, J., Torres, M.R. and Tornero, J.D. (1997) Molecular Structure of a Unique UV Stabilizer: Tinuvin P. *Journal of the Chemical Society, Faraday Transactions*, **93**, 1691-1696. https://doi.org/10.1039/A607652A

[37] Zhurko, G. and Zhurko, D. (2013) Chemcraft (Version 1.7, Build 375, 2013).

[38] Jin, R. (2010) A DFT Study on the Radical Scavenging Activity of Juglone and Its Derivatives. *Journal of Molecular Structure: THEOCHEM*, **939**, 9-13. https://doi.org/10.1016/j.theochem.2009.09.024

[39] Alisi, I.O., Uzairu, A. and Abechi, S.E. (2019) *In Silico* Design of Hydrazone Antioxidants and Analysis of Their Free Radical-Scavenging Mechanism by Thermodynamic Studies. *Beni-Suef University Journal of Basic and Applied Sciences*, **8**, Article No. 11. https://doi.org/10.1186/s43088-019-0011-2

[40] Özbakır Işın, D. (2016) Theoretical Study on the Investigation of Antioxidant Properties of Some Hydroxyanthraquinones. *Molecular Physics*, **114**, 3578-3588. https://doi.org/10.1080/00268976.2016.1248514

[41] Mikulski, D., Eder, K. and Molski, M. (2014) Quantum-Chemical Study on Relationship between Structure and Antioxidant Properties of Hepatoprotective Compounds Occurring in *Cynara scolymus* and *Silybum marianum*. *Journal of Theoretical and Computational Chemistry*, **13**, Article ID: 1450004. https://doi.org/10.1142/S0219633614500047

[42] Farmanzadeh, D. and Najafi, M. (2013) On the Antioxidant Activity of the Tryptophan Derivatives. *Bulletin of the Chemical Society of Japan*, **86**, 1041-1050. https://doi.org/10.1246/bcsj.20130035

[43] Fouegue, A.D.T., Mama, D.B., Ghogomu, J.N., Elie, Y. and Etoh, M.A. (2018) The Substitution Effect on Reaction Enthalpies of Antioxidant Mechanisms of Juglone and Its Derivatives in Gas and Solution Phase: DFT Study. *Journal of Chemistry*, **2018**, Article ID: 1958047. https://doi.org/10.1155/2018/1958047

[44] Akhtari, K., Hassanzadeh, K., Fakhraei, B., Fakhraei, N., Hassanzadeh, H. and Zarei, S.A. (2013) A Density Functional Theory Study of the Reactivity Descriptors and Antioxidant Behavior of Crocin. *Computational and Theoretical Chemistry*, **1013**, 123-129. https://doi.org/10.1016/j.comptc.2013.03.015

[45] Najafi, M., Najafi, M. and Najafi, H. (2012) DFT/B3LYP Study of the Substituent Effects on the Reaction Enthalpies of the Antioxidant Mechanisms of Magnolol Derivatives in the Gas-Phase and Water. *Bulletin of the Korean Chemical Society*, **33**, 3607-3617. https://doi.org/10.5012/bkcs.2012.33.11.3607

[46] Mishra, A., Verma, C., Srivastava, V., Lgaz, H., Quraishi, M., Ebenso, E.E. and Chung, I.-M. (2018) Chemical, Electrochemical and Computational Studies of Newly Synthesized Novel and Environmental Friendly Heterocyclic Compounds as Corrosion Inhibitors for Mild Steel in Acidic Medium. *Journal of Bio- and Tribo-Corrosion*, **4**, Article No. 32. https://doi.org/10.1007/s40735-018-0147-y

[47] Obot, I., Kaya, S., Kaya, C. and B. Tüzün (2016) Density Functional Theory (DFT) Modeling and Monte Carlo Simulation Assessment of Inhibition Performance of Some Carbohydrazide Schiff Bases for Steel Corrosion. *Physica E*: *Low-Dimensional Systems and Nanostructures*, **80**, 82-90. https://doi.org/10.1016/j.physe.2016.01.024

Supplementary Information

Table S1. Selected gas-phase computed bond lengths and angles of PBT **Table S1.**

Bond type	Bond lengths[a] (Å)		Bond type	Bond angles[a] (˚)	
	Expt[b].	Compt[c].		Expt[b].	Compt[c].
C1-C2	1.407	1.401	C2-C3-C4	121.1	120.9
C2-C3	1.402	1.421	C6-C1-C2	116.1	116.9
C3-C4	1.404	1.401	C4-C5-C6	121.8	121.9
C4-C5	1.361	1.374	C5-C6-C1	122.8	122.0
C5-C6	1.409	1.414	C5-C4-C3	116.8	117.1
C6-C1	1.358	1.374	C2-C3-N13	109.2	108.7
C2-N11	1.349	1.348	N11-C2-C1	130.3	131.0
C3-N13	1.352	1.350	N13-C3-C2	109.2	108.7
N11-N12	1.340	1.341	N12-N13-C3	102.8	103.5
N12-N13	1.330	1.326	N12-N11-C2	103.2	103.8
N12-C14	1.430	1.415	N12-C14-C15	120.5	120.6
C14-C15	1.398	1.408	C14-C15-O16	124.6	124.6
C14-C20	1.385	1.394	C15-C17-C18	121.0	121.3
C15-O16	1.361	1.343	C17-C18-C19	121.7	121.5
C15-C17	1.383	1.396	C18-C19-C20	116.9	117.8
C17-C18	1.379	1.377	C19-C20-C14	122.3	121.4
C18-C19	1.392	1.398	C20-C14-C15	120.1	120.6
C19-C20	1.380	1.382	C18-C19-C25	121.2	121.1
C19-C25	1.499	1.498			

[a]Refer to **Figure 1** for atom numbering. [b]Experimental values of selected bond lengths and angles. [c]Computed values of selected bond lengths and angles from this work using the B97-3c method.

Table S2. Enthalpies (in kJ/mol) of the electron $H(e^-)$, proton $H(H^+)$ and hydrogen atom $H(H^\cdot)$ used in this study at the M06-2x/6-311++G(d,p) level of theory.

Medium	Electron	Proton	H-atom
Gas	3.146	6.197	−1301.81
Water	−77.5	−1055.7	−1296.26

Table S3. Enthalpies (in kJ/mol) of the neutral molecules $H(BTOH)$ used in this studied as computed at the M06-2x/6-311++G(d,p) level of theory.

Species	Gas	Water
Phenol	−806,850.3	−806,877.0
PBT	−1,945,828.3	−1,945,852.8
PBT1	−2,091,120.0	−2,091,155.6
PBT2	−2,187,994.2	−2,188,027.5

Table S4. Enthalpies (in kJ/mol) of the radical species $H(BTO^{\bullet})$ of the molecules under investigation used in this studied as computed at the M06-2x/6-311++G(d,p) level of theory.

Species	Gas	Water
Phenol	−805,176.3	−805,204.1
PBT	−1,944,128.5	−1,944,179.6
PBT1	−2,089,462.1	−2,089,528.2
PBT2	−2,186,288.4	−2,186,345.7

Table S5. Enthalpies (in kJ/mol) of the cationic radical species $H(BTOH^{\bullet+})$ of the molecules under investigation used in this studied as computed at the M06-2x/6-311++G(d,p) level of theory.

Species	Gas	Water
Phenol	−806,027.6	−806,278.5
PBT	−1,945,071.9	−1,945,265.8
PBT1	−2,090,429.5	−2,090,634.8
PBT2	−2,187,192.3	−2,187,410.6

Table S6. Enthalpies (in kJ/mol) of the anionic species $H(BTO^{-})$ of the molecules under investigation used in this studied as computed at the M06-2x/6-311++G(d,p) level of theory.

Species	Gas	Water
Phenol	−805,403.3	−805,669.0
PBT	−1,944,395.3	−1,944,647.2
PBT1	−2,089,693.6	−2,089,947.0
PBT2	−2,186,621.1	−2,186,853.3

Table S7. Cartesian coordinates of the gas phase optimised geometry of neutral form of **PBT**.

28			
C	−3.05591541934523	1.95647880674736	0.18111160950319
C	−1.84501303234037	1.31304728403805	0.46665934216414
C	−1.78913919457020	−0.08963588248016	0.68527513644604
C	−2.94828738478569	−0.87472160647401	0.62179918183079
C	−4.12731004505138	−0.22818767746071	0.34070160062671
C	−4.18016746315908	1.16841394789389	0.12345326059736
H	−3.09807448663761	3.02332016671571	0.01482466629639
H	−2.90635820495959	−1.94148479712858	0.78796218738119
H	−5.04477250661527	−0.79752648706695	0.28258553664493
H	−5.13631054696681	1.62412877846508	−0.09426844268632

Continued

N	−0.59278829570219	1.79768711944128	0.58974806961426
N	0.14427538092935	0.71252330440437	0.86739229309917
N	−0.50941711403224	−0.43886920776529	0.93735002645170
C	1.54114616696257	0.80631464137856	1.07083382375431
C	2.19593416683032	2.05070579237899	0.99212061649174
O	1.58566147287528	3.21759349610530	0.72690596178347
C	3.57443498583423	2.06682363046205	1.21082270436012
C	4.26764496102337	0.91033964867431	1.49167890947933
C	3.62160988441622	−0.32766938086238	1.56717894898357
C	2.25638645674016	−0.35584791456177	1.35536644338310
H	1.71147576017589	−1.28594259037537	1.40761844181401
H	0.62294440502394	3.02687624161699	0.60262577312658
H	4.07637879969605	3.02210217145785	1.15650855493710
H	5.33616750313068	0.96477040713231	1.65874099073661
C	4.38847573547735	−1.58426477460963	1.84203787124110
H	3.73611858790326	−2.38209403542508	2.18957891152585
H	4.89383007695634	−1.94452498902262	0.94426343652391
H	5.15548934019067	−1.42536609367957	2.59864431388954

Table S8. Cartesian coordinates of the gas phase optimised geometry of neutral form of **PBT1**.

30			
C	−2.94766282028705	2.02648018458478	0.19831926100417
C	−1.75570404782677	1.35126528965663	0.48957371737747
C	−1.73582664485798	−0.05418931976300	0.69348551118245
C	−2.91255193731574	−0.81044227577829	0.60919763034913
C	−4.07306415983764	−0.13309198252665	0.32257593449206
C	−4.09005903531459	1.26626339973678	0.12003823591484
H	−2.96312272759841	3.09587998800420	0.04376904841125
H	−2.89791082508299	−1.87958258580423	0.76450072174093
H	−5.00321637420174	−0.67971032207986	0.24871560727256
H	−5.03268503213624	1.74735267889062	−0.10248941910324
N	−0.49316128481596	1.80347686192932	0.63144907665784
N	0.21474560807769	0.69748981225958	0.90593014101485
N	−0.46769574556743	−0.43730600430570	0.95597642536766
C	1.61174322529550	0.75223855667562	1.12415431770585
C	2.27987148120655	1.98005943812133	1.07676639455490
O	1.69754228485564	3.17237510274062	0.82273247224273

Continued

C	3.67378385364703	1.99701276135296	1.29071270103694
C	4.33495186522886	0.80542435891041	1.54405078082654
C	3.66281435627999	−0.41756769763319	1.59076028273350
C	2.29852773503055	−0.43635127521715	1.38411958796984
H	1.74252933028501	−1.35940648825139	1.41386340336209
H	0.73351612352166	2.99907295002790	0.67423209685579
H	5.40527751123971	0.83153443164043	1.71482578157341
C	4.41876543030049	−1.68254437312243	1.85984566803855
H	3.75073325899644	−2.53816611150733	1.91910935004764
H	5.14745346845345	−1.88558884103078	1.07387254242035
H	4.97002026723605	−1.62525654371952	2.79886465453390
N	4.31598956615426	3.22484343394664	1.30680257391063
H	3.81701021424400	3.95269597730320	0.82231835432913
H	5.28883505478966	3.19469859495850	1.05324714617623

Table S9. Cartesian coordinates of the gas phase optimised geometry of neutral form of **PBT2**.

29			
C	−3.01910505381941	1.97527437712061	0.18610123592083
C	−1.81443733202107	1.31889046928475	0.47122741528945
C	−1.77097728944808	−0.08612839715577	0.68292320302841
C	−2.93685273866720	−0.86161357975385	0.61285039689658
C	−4.10809811935556	−0.20257999559047	0.33261309408181
C	−4.14839476872109	1.19652598713108	0.12226453232015
H	−3.05170468882404	3.04310313711462	0.02526976512964
H	−2.90476228299184	−1.92938557902307	0.77358999205479
H	−5.03074192786794	−0.76276858747401	0.26935496706957
H	−5.10038528604872	1.66081466756971	−0.09508920874691
N	−0.55898474253612	1.79133195923726	0.59976089518870
N	0.16715191879058	0.69793579302529	0.87342415183469
N	−0.49560828593910	−0.44811182410881	0.93613535957497
C	1.56407276613851	0.77772541672341	1.08083416376983
C	2.22185515491296	2.02050047615200	1.00648120095197
O	1.62148373164474	3.18126930896212	0.74524940927613
C	3.61280293415542	2.02547934537998	1.23099868028155
C	4.29516987700522	0.84446155260570	1.51200127190174
C	3.63574033631295	−0.37666077342604	1.57864909836813
C	2.26676219533413	−0.38791777809049	1.36249715267377

Continued

H	1.71286058390979	−1.31297673550248	1.41017708417538
H	0.65472194590764	2.99481378106587	0.61832987217556
H	5.36180624173223	0.89603482884650	1.68078291231911
C	4.38458955031283	−1.64516420348689	1.84882014509548
H	3.73465507926669	−2.40945381082670	2.26821837004751
H	4.81464566041381	−2.05032555600170	0.93168653846849
H	5.20501756884774	−1.48208070437908	2.54472423137782
C	4.32015809686897	3.25127712478696	1.17561288125592
N	4.93329887468593	4.23512929981342	1.13963118821889

Table S10. Cartesian coordinates of the gas phase optimised geometry of **PBT** radical.

27			
C	−2.95333269173909	1.74898350608147	−0.34206885994238
C	−1.79014573654181	1.22307404000858	0.24553283467541
C	−1.82621056525776	0.00165709054688	0.98412343728246
C	−3.02950912413525	−0.70345107751926	1.15397086215762
C	−4.15057721561081	−0.16996438889539	0.57293491226653
C	−4.11356416051472	1.04175141563141	−0.16630868032711
H	−2.92326104797585	2.67379654314569	−0.89976873538339
H	−3.06095674196065	−1.62458194089072	1.71810182724924
H	−5.09763108551453	−0.68185952989114	0.67765798178955
H	−5.03342513822122	1.41177036813396	−0.59822383517486
N	−0.53107185354448	1.68799326992028	0.24140166235750
N	0.12465983174735	0.76993728598280	0.95710521998348
N	−0.58666809997206	−0.26973275315448	1.42315824197017
C	1.50819843079702	0.83984576202200	1.16292253195775
C	2.15492585639130	2.14066208533334	1.35426434139206
O	1.53120260973849	3.20979151776304	1.47181925731569
C	3.59655259328984	2.09161817565719	1.47612331457752
C	4.28055171925014	0.91643755870721	1.52420976003788
C	3.61175432312103	−0.32425316013019	1.41593444357443
C	2.22916723708456	−0.33082345083492	1.23382807301429
H	1.70262465385125	−1.26839005309881	1.13066946435931
H	4.09431296097195	3.04547660631743	1.57598267025652
H	5.35689883566908	0.92042509535960	1.64735017009994
C	4.37961371139903	−1.59842860309602	1.49185054700550
H	3.76819986657590	−2.45800692410345	1.23219849297199
H	5.24560870724612	−1.57905742948025	0.83002624832809
H	4.76356212385515	−1.75656100951627	2.50209381620474

Table S11. Cartesian coordinates of the gas phase optimised geometry of **PBT1** radical.

29			
C	−3.05458470160153	1.92765858976904	0.94835684820104
C	−1.79650497818080	1.31378944633886	0.84041154782556
C	−1.66850871307665	−0.01651634981829	0.34677826760822
C	−2.79744988018331	−0.74936454273257	−0.05297213979047
C	−4.01640970355543	−0.12993370546230	0.06068839499912
C	−4.14392839584126	1.19232585986556	0.55574569923467
H	−3.14920743997402	2.93710905249293	1.32224768465664
H	−2.70198421282288	−1.75666930734280	−0.43297524163904
H	−4.91150355858208	−0.66008442844466	−0.23587749050070
H	−5.13188714746371	1.62785565278673	0.62093165104266
N	−0.57107040527842	1.77888260252147	1.14574955263696
N	0.21959382672533	0.75575659467538	0.82794037902012
N	−0.36466616834294	−0.35088739454516	0.35134400509916
C	1.61205531244967	0.79683673128629	1.04633228363515
C	2.34602887870061	1.99570042837429	0.70283628167634
O	1.87070626907719	3.00662009627659	0.15481295940671
C	3.78925989829092	1.94294401117844	1.00102312203817
C	4.38747967213431	0.78882458567069	1.49727066400933
C	3.63499418901651	−0.34381330680275	1.74989852254125
C	2.24244490920756	−0.32015442397233	1.52101736279456
H	1.65186257641958	−1.20137934883948	1.72622944430792
H	5.45431225165721	0.77900679021730	1.68795364141538
C	4.26414321623756	−1.59035356047991	2.27709927415883
H	4.10913984634618	−2.42602657118213	1.59323165358796
H	5.33412663956379	−1.47117340559678	2.42571975945432
H	3.82167253567494	−1.88084445861333	3.23084115423379
N	4.45160683813609	3.08181607683339	0.74209202712655
H	3.92327560157359	3.80663601279452	0.27929050478964
H	5.45293284369192	3.12531827275096	0.74308218643011

Table S12. Cartesian coordinates of the gas phase optimised geometry of **PBT2** radical.

28			
C	−3.09862244673129	1.92651902981970	0.78683406252558
C	−1.84105142137041	1.29961441818655	0.74061444031888
C	−1.71801447648128	−0.08271584812448	0.39706835028972
C	−2.85155152159610	−0.85198600460188	0.08328273883643
C	−4.06480645206162	−0.21784011524652	0.13376633272925

Continued

C	−4.18755213421450	1.15498042477000	0.48111070287808
H	−3.18804729649483	2.97131626645434	1.04612421917260
H	−2.76133527823090	−1.89507616706838	−0.18349680492655
H	−4.96364921461538	−0.77266227569966	−0.09826898951279
H	−5.17467214329047	1.59599672384840	0.49937853876246
N	−0.61938350998240	1.79402132952760	0.98575151175934
N	0.17295079606421	0.73593380196760	0.78290381250769
N	−0.42064118325891	−0.42055512289017	0.43886479105798
C	1.55433168718115	0.79309998386273	0.98768100984780
C	2.28001497338554	2.02776848154625	0.67235207197156
O	1.77314052114630	2.99889566344758	0.10428867075031
C	3.70825271373771	1.99470554223612	1.01363809321166
C	4.31547484353635	0.84725714727063	1.46463858176893
C	3.58531765522023	−0.33622858306383	1.66341743566641
C	2.21011457301288	−0.33536416549878	1.41957308403111
H	1.63408315901964	−1.23409560219583	1.58408441844891
H	5.37804694052520	0.85542822677548	1.66739057018141
C	4.26519183102217	−1.55735106553856	2.17953419901750
H	3.67469876969890	−2.45233764043363	2.00450824087381
H	5.24331856588061	−1.69112113982722	1.72058914486499
H	4.43096389593128	−1.47841653866483	3.25641654263802
C	4.46274696337592	3.17004834184893	0.80986168182638
N	5.11270918958994	4.12074488729182	0.66486254850241

Table S13. Cartesian coordinates of the gas phase optimised geometry of **PBT** cationic radical.

28			
C	−3.03362340591211	1.98680977576712	0.18928645882103
C	−1.83325048441812	1.32379838597749	0.47217802224838
C	−1.79731419063745	−0.09931751770172	0.69356307271014
C	−2.97183772918257	−0.87306092307512	0.63259635521362
C	−4.12940856369712	−0.20447671646477	0.35527016385007
C	−4.15943593021818	1.20689673487365	0.13656142531903
H	−3.06635089181939	3.05278142519210	0.02257816158186
H	−2.94452809442709	−1.93916740881696	0.79850338160791
H	−5.05976137969944	−0.75034979268066	0.29674201766132
H	−5.11192895501489	1.66963947722362	−0.07836038522363
N	−0.58019120427797	1.78257574019810	0.59282127629760

Continued

N	0.14315446031144	0.67775359236556	0.87022563793939
N	−0.53767071453062	−0.47149799914330	0.94129632838533
C	1.51455404143897	0.74586670328682	1.06801267965097
C	2.18529495583267	2.02349272188678	0.97618821951162
O	1.56173253199231	3.13977739290071	0.71209847819793
C	3.58054618455696	2.06767624586783	1.18152765490840
C	4.26722555224410	0.92671120040044	1.45880231685109
C	3.61180014808693	−0.33698758142496	1.55069435920932
C	2.24014478161936	−0.39820700552146	1.35156158050373
H	1.71768330370075	−1.33959390701594	1.41486496061962
H	0.57436295149224	2.93148036604182	0.59342675455312
H	4.06633461880944	3.02901662197934	1.10963216147672
H	5.33628856016099	0.97066927758624	1.61459240970442
C	4.40277768254067	−1.55137116795020	1.85478915013890
H	3.79100351532538	−2.44581907775602	1.89890663332839
H	5.18162703386560	−1.69980058491200	1.10395203814963
H	4.92519121185717	−1.44030597908458	2.80720885678397

Table S14. Cartesian coordinates of the gas phase optimised geometry of **PBT1** cationic radical.

30			
C	−2.92631679657965	2.04954817260304	0.19567262237572
C	−1.74236932493332	1.35272802176867	0.47690998385092
C	−1.73904452018544	−0.06504724702717	0.65948359625533
C	−2.92477504210929	−0.80872171165318	0.56293881340222
C	−4.06994034721000	−0.10917198690115	0.28765376508465
C	−4.06961309763592	1.29914920031210	0.10686613983241
H	−2.93284220871500	3.12032307733944	0.05714346746693
H	−2.92311554732839	−1.87941257804194	0.70070867081158
H	−5.00815062139716	−0.63842220638238	0.20368484077336
H	−5.00786300355897	1.79020979479073	−0.10813500798932
N	−0.47671118172747	1.78005874378201	0.62716185149165
N	0.21631074935743	0.65152917585698	0.88422743717103
N	−0.47999133838461	−0.47105607743474	0.91564593445130
C	1.60199370751439	0.70212098429969	1.10231600510446
C	2.25543178480896	1.95580967966338	1.04719776534548
O	1.65312656791766	3.09320843079971	0.80347152035538
C	3.68223126857462	1.99765990487352	1.27303790690566

Continued

C	4.38077488997942	0.81146206728463	1.53885127325867
C	3.72325974938998	−0.39448368130699	1.58726664486861
C	2.32079048743401	−0.43755261828663	1.36538391018286
H	1.79880058233715	−1.38167869376241	1.40198137058725
H	0.64966584621900	2.87439364167694	0.66908245626702
H	5.44796014069699	0.85726429241516	1.70595010885163
C	4.44055923823745	−1.66654908031582	1.86729168294625
H	4.03239125494105	−2.15149217981124	2.75462589743208
H	4.31176448523439	−2.37028292863138	1.04428605650968
H	5.50332432571517	−1.51142667494974	2.02110926234979
N	4.27390537622799	3.19197007471664	1.21541128089554
H	3.73649213280033	4.02140857310086	1.02174248794421
H	5.26340044237916	3.29541382922125	1.36235225521764

Table S15. Cartesian coordinates of the gas phase optimised geometry of **PBT2** cationic radical.

29			
C	−2.99121726049464	2.00735003566068	0.19741842545736
C	−1.80065782010895	1.33394434284265	0.47866495210380
C	−1.77766009587501	−0.09049846503251	0.69179467330546
C	−2.96093438617254	−0.85611105499994	0.62339746645479
C	−4.11156952895674	−0.17724108256723	0.34753615594132
C	−4.12667282267562	1.23470289221306	0.13745377208851
H	−3.01701355997279	3.07438228656085	0.03645257388037
H	−2.94100737124012	−1.92326937126645	0.78346233802948
H	−5.04682328110815	−0.71376460634606	0.28342311127520
H	−5.07366659124998	1.70879638582146	−0.07716588508976
N	−0.54015718991212	1.77928242090269	0.60607616417246
N	0.16923712900211	0.67001015066465	0.87788952848084
N	−0.52466146854005	−0.47675790273709	0.94040722255974
C	1.54208875914157	0.71842796232284	1.08101499499121
C	2.21609372923572	1.98950118147467	0.99729791592094
O	1.60423945864592	3.10645407309911	0.73927744195500
C	3.62777063681106	2.01948222573829	1.20913930337583
C	4.29895664987274	0.85238110671482	1.48359154059384
C	3.62775972261292	−0.39234934002777	1.56383421094396
C	2.25360820688867	−0.43433774379189	1.35952703499048
H	1.72033293824629	−1.37017835866019	1.41549571780753

Continued

H	0.61109880109182	2.90497674850425	0.61676812292719
H	5.36717649065407	0.88925544242165	1.64180689137461
C	4.40045509193420	−1.62129157979813	1.86289683204565
H	3.77360394959684	−2.50557295647748	1.89739171754940
H	5.17931495768801	−1.77712465238623	1.11400617253019
H	4.91886644854781	−1.52599267704876	2.81888283874525
C	4.30142366860104	3.26043711776337	1.12979884645179
N	4.86675473773587	4.27050541843461	1.06757991913748

Table S16. Cartesian coordinates of the gas phase optimised geometry of the anionic form of **PBT**.

27			
C	−2.96457552809545	1.71813826549758	−0.36244382439448
C	−1.79394156340737	1.22144916162905	0.22349266513345
C	−1.81428520818339	0.02409225884734	0.99236657570215
C	−3.00803303809804	−0.68396132941795	1.18261212666825
C	−4.15191988312790	−0.17826476995464	0.59902543640672
C	−4.13038925022039	1.00622390541892	−0.16673447307182
H	−2.94567149089040	2.62991426811387	−0.94458448271000
H	−3.02627687477200	−1.59265504719725	1.77043023002555
H	−5.09209015744976	−0.70059897145402	0.72971441352790
H	−5.05384056861833	1.36300195799587	−0.60654810936375
N	−0.52913316840248	1.68963931006364	0.18869244145431
N	0.14519077542353	0.80598706204138	0.92477996500788
N	−0.56592624388758	−0.21676454311131	1.43957393617201
C	1.53398314617422	0.89955549736099	1.13382953361176
C	2.16240774929826	2.19743415347863	1.34142734338873
O	1.56629277408794	3.29825238870101	1.37990597019757
C	3.58933258583345	2.08691634590506	1.55341539586775
C	4.26349009980439	0.89663744312143	1.59679146715818
C	3.60772313254958	−0.33786276030929	1.42624487731429
C	2.24563151251619	−0.29770699565560	1.20518260016767
H	1.69386782821873	−1.21933551702712	1.06872192170718
H	4.11033363356440	3.02510401352343	1.70217917851387
H	5.33850445342767	0.90105900649636	1.76562146999595
C	4.36415889793349	−1.63019056505919	1.46077774066048
H	3.69026723793457	−2.48114523458475	1.36304604689337
H	5.09954972268367	−1.70634614473585	0.65295620842336
H	4.91682942570294	−1.76046315968762	2.39641334554160

Table S17. Cartesian coordinates of the gas phase optimised geometry of the anionic form of **PBT1**.

29			
C	−3.06099652319668	1.94697456226706	0.79520863954266
C	−1.79999241583615	1.33906907931983	0.77610890995638
C	−1.65238034823242	−0.02231783258194	0.38913728545066
C	−2.76644682097183	−0.78482780886415	0.01597078527932
C	−4.00166004612240	−0.16812475113848	0.03919144739223
C	−4.14795604020703	1.17970148247373	0.42683960600691
H	−3.16913887466313	2.98282395297726	1.08846734917532
H	−2.65574344573791	−1.81948477307294	−0.28218184684678
H	−4.88278891956323	−0.73011260036414	−0.24661508633144
H	−5.13784523150527	1.61980711664806	0.43134010530328
N	−0.58489461598030	1.83091175391381	1.09482040881934
N	0.23139279667267	0.79751970791942	0.87815231217537
N	−0.34526677377062	−0.34452555298730	0.45251959578446
C	1.61608801031470	0.85818251852562	1.11755218027196
C	2.33916894155856	2.07499275325420	0.87880578510921
O	1.87804912110977	3.15912095570727	0.42709890195503
C	3.77256356027699	1.96868849388645	1.14796691427479
C	4.35967159963149	0.79606262019562	1.54796890068630
C	3.60690598854439	−0.38298906538045	1.73321724439683
C	2.25160784750287	−0.33062301843979	1.51217729961417
H	1.64062646886493	−1.21213329910089	1.64822978399330
H	5.43123581982888	0.77625109870078	1.73713319466993
C	4.27731986896745	−1.64221677124638	2.18874694259525
H	3.56377448054820	−2.46287016683473	2.25686831580545
H	5.07186701863013	−1.95628364195314	1.50429655737327
H	4.74236307929998	−1.53189719978442	3.17378838771974
N	4.47185525840861	3.16759426823435	0.97481165767601
H	3.85471034623203	3.79936898788729	0.46937712540930
H	5.35383984939531	3.05121712983798	0.50010129674171

Table S18. Cartesian coordinates of the gas phase optimised geometry of the anionic form of **PBT2**.

28			
C	−2.90678025707820	1.63003537126730	−0.50431023721673
C	−1.75469296544486	1.16876394218512	0.14619351197600
C	−1.81483500398241	0.07002204610607	1.04779845303852

Continued

C	−3.03034810545064	−0.57730397530762	1.30955168052773
C	−4.15182679841722	−0.10918297261247	0.66144115461421
C	−4.09086292372915	0.97999538138691	−0.23668092349078
H	−2.85756219202597	2.46792523954964	−1.18642902737294
H	−3.07901090611893	−1.40998210363521	1.99876368528368
H	−5.10836628928912	−0.58374241383448	0.84253255860593
H	−5.00172579909423	1.30969671800949	−0.72066904638046
N	−0.47659019350837	1.59286387408890	0.07107855186471
N	0.16132791813330	0.77991023550633	0.90739478004089
N	−0.57548400745566	−0.15508693858006	1.52836438963665
C	1.55763808950647	0.86043251614133	1.11379820532550
C	2.16866954191349	2.16767814975916	1.33748720926482
O	1.54466535068875	3.23974089389604	1.39430028816647
C	3.61324766937282	2.06402556904408	1.53709708380138
C	4.28680630760669	0.84426984039456	1.55843935772025
C	3.63567446232966	−0.36803569513949	1.38306407819448
C	2.25913781441391	−0.32523138824920	1.16593711835287
H	1.70772819104077	−1.24703083579486	1.02407189713651
H	5.35916580333231	0.85383480857915	1.72186576638486
C	4.37703117374256	−1.67067194023703	1.38331974465566
H	3.89297492236622	−2.41455020770943	2.01959833626948
H	4.44882057673692	−2.10948937304700	0.38361578530193
H	5.39518446339706	−1.54110422873288	1.74944017300732
C	4.34958427187074	3.24727100065207	1.74644898278875
N	5.00245888514306	4.19552648631351	1.92325644250224

Table S19. Cartesian coordinates of the gas phase optimised geometry of neutral form of **Phenol**.

13			
C	−2.45237451593595	1.93997528076273	−0.02582868805402
C	−1.37143501821014	1.06618284807096	0.03876897963578
C	−1.59124536634413	−0.30272471290742	0.07701304743363
C	−2.88169589721732	−0.81026242626601	0.05146735356627
C	−3.95530919532794	0.06904195554530	−0.01305603553135
C	−3.74949437440624	1.43757943509676	−0.05172546405231
O	−2.30231036148416	3.29787797496739	−0.06610047861539
H	−1.36207586605782	3.50951261975985	−0.04184979507995
H	−0.35961296280297	1.45532624202775	0.05904339577356

Continued

H	−0.74404804430274	−0.97391271995898	0.12715709031594
H	−3.04953988813392	−1.87783137601883	0.08140296612123
H	−4.96736389853680	−0.31327430682404	−0.03357889547072
H	−4.57890461123984	2.12888918574453	−0.10192347604266

Table S20. Cartesian coordinates of the gas phase optimised geometry of **Phenolic** radical.

12			
C	−2.73501820878967	1.95284375076834	−0.05123045197369
C	−1.54030629905145	1.14055608169042	0.01552096708406
C	−1.62110259626482	−0.22483218188952	0.07551306878256
C	−2.87019080512006	−0.86013741109789	0.07304761718924
C	−4.05284862911457	−0.11101224250475	0.00941817441481
C	−4.00225706548446	1.25574381809561	−0.05136676246012
O	−2.67500216955296	3.20504937560642	−0.10648800097934
H	−0.59161075538656	1.65862423169207	0.01579403940128
H	−0.72056359422903	−0.82304335033478	0.12530581315976
H	−2.92189493024017	−1.93929478834737	0.12075953867259
H	−5.00663486777962	−0.62247012297721	0.00873272848750
H	−4.89667007898662	1.86070283929867	−0.10123673177866

Table S21. Cartesian coordinates of the gas phase optimised geometry of **Phenolic** cationic radical.

13			
C	−2.44315136906674	1.93137544502077	−0.02517593041211
C	−1.32791860659219	1.04975653553256	0.04079854115914
C	−1.55768458128042	−0.29379458096829	0.07780587073701
C	−2.88268984066563	−0.78789227966623	0.05067371434882
C	−3.98469168653452	0.08677297030023	−0.01462523792434
C	−3.78093838209409	1.43524177822578	−0.05265117099545
O	−2.31685148630923	3.23777666054159	−0.06446838214934
H	−1.38805082003616	3.52763593674504	−0.04355576590399
H	−0.32270445769015	1.44989553439018	0.06054004704033
H	−0.73088387265492	−0.98680857928878	0.12797810929560
H	−3.04961371092455	−1.85516123766835	0.08064186902499
H	−4.98721557005567	−0.31397890481796	−0.03425601034227
H	−4.59301561609569	2.14556072165345	−0.10291565387841

Table S22. Cartesian coordinates of the gas phase optimised geometry of the **Phenolic** anion.

12			
C	−2.44526909142647	2.02923402858075	−0.02855701739006
C	−1.37455411532344	1.06595695302561	0.03863837711111
C	−1.59651996766629	−0.29693082675364	0.07662704168464
C	−2.88671236088660	−0.83106402578279	0.05203232711885
C	−3.95650147407949	0.06466993803139	−0.01295241904460
C	−3.75712937317494	1.43083086429520	−0.05177867455199
O	−2.25236125646454	3.28281722307097	−0.06386231270575
H	−0.36229899640274	1.45791673313500	0.05884008078921
H	−0.74280522296212	−0.97080693870963	0.12708522321310
H	−3.05204749824726	−1.90202068007519	0.08215199417783
H	−4.97379653113973	−0.32284738129657	−0.03346020369565
H	−4.60333411222638	2.10913411247891	−0.10213441670671

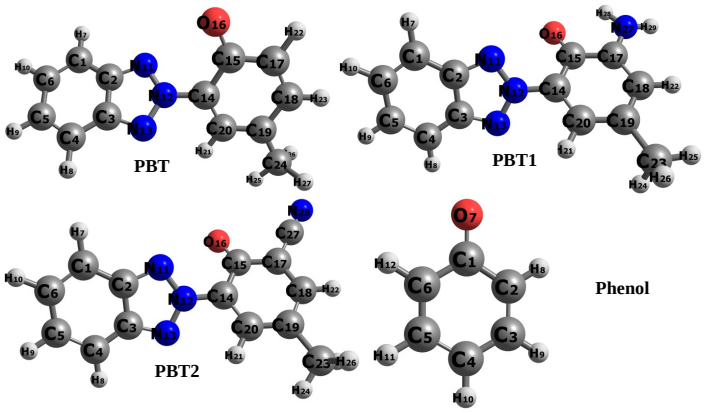

Figure S1. Optimized structures of the radicals of the studied compounds obtained from B97-3c calculations in gas phase.

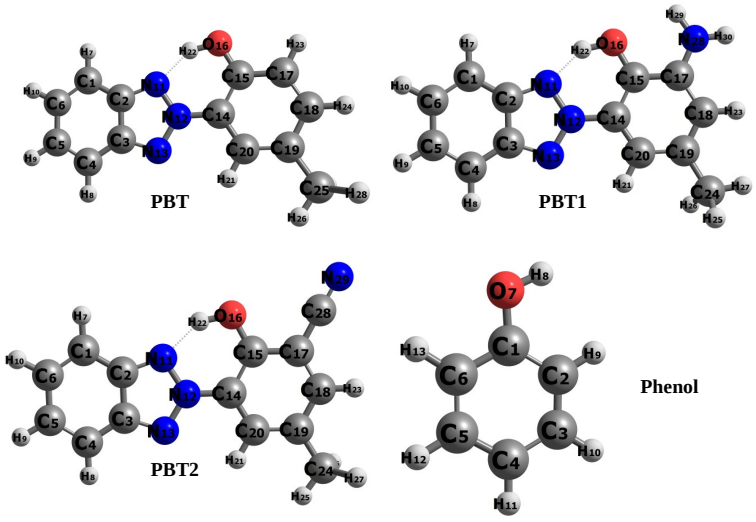

Figure S2. Optimized structures of the cationic radicals of the studied compounds obtained from B97-3c calculations in gas phase.

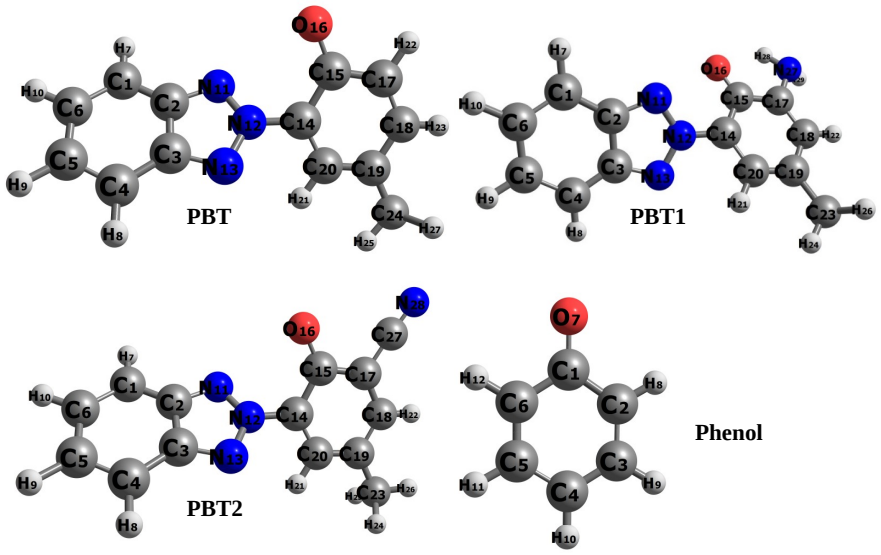

Figure S3. Optimized structures of the anionic forms of the studied compounds obtained from B97-3c calculations in gas phase.